nature cell biology

Active diffusion positions the nucleus in mouse oocytes

Maria Almonacid[1,7], Wylie W. Ahmed[2,3,4,7], Matthias Bussonnier[2,3,4], Philippe Mailly[1], Timo Betz[2,3,4], Raphaël Voituriez[5], Nir S. Gov[6] and Marie-Hélène Verlhac[1,8]

In somatic cells, the position of the cell centroid is dictated by the centrosome. The centrosome is instrumental in nucleus positioning, the two structures being physically connected. Mouse oocytes have no centrosomes, yet harbour centrally located nuclei. We demonstrate how oocytes define their geometric centre in the absence of centrosomes. Using live imaging of oocytes, knockout for the formin 2 actin nucleator, with off-centred nuclei, together with optical trapping and modelling, we discover an unprecedented mode of nucleus positioning. We document how active diffusion of actin-coated vesicles, driven by myosin Vb, generates a pressure gradient and a propulsion force sufficient to move the oocyte nucleus. It promotes fluidization of the cytoplasm, contributing to nucleus directional movement towards the centre. Our results highlight the potential of active diffusion, a prominent source of intracellular transport, able to move large organelles such as nuclei, providing *in vivo* evidence of its biological function.

Cells sense their geometry to adapt their polarity to forces exerted by the environment. Centrosome location constitutes an excellent cell geometry sensor. Centrosomes regulate cell shape, polarity, intracellular transport and positioning of compartments[1]. In many cells, the centrosome is positioned at the cell centroid by its radiating microtubules that contact the cortex[2,3]. Centrosome location also regulates nucleus position, the two structures being physically connected[4–6]. Importantly, nucleus position is involved in many functions and abnormal positioning can lead to dysfunction and disease[7]. The location of the nucleus harbours instructive function and can be regulated during the life of the cell. This is the case for the developing vertebrate neuroepithelium, where nucleus position depends on the cell cycle stage.

Different mechanisms account for nucleus movement including microtubule polymerization, as for the worm male pronucleus migration of the zygote, actin polymerization, playing a role in nucleus positioning in *Drosophila* nurse cells[8], or actin flows occurring in migrating cells[7,9]. In a variety of species, the location of the oocyte nucleus defines the future axis of the embryo. In worms, sea urchin, frog, some fishes and amphibians, the nucleus marks the location of the animal pole. In the *Drosophila* oocyte the nucleus determines the dorsoanterior axis of the future embryo[10].

Mouse oocytes have unique properties. First, as for most oocytes, these large cells (80 μm wide) lack canonical centrosomes: centrioles are lost during late oogenesis, before follicle growth[11]. Second, differently from many species, these cells show no sign of polarization before meiosis resumption and as they exit meiosis become isolated from extracellular inputs[12]. Despite that, mouse oocytes exhibit an almost perfect spherical symmetry with their large nuclei (30 μm wide) at the centre, suggesting that even without canonical centrosomes they can find their geometric centre. We decided to investigate this mechanism, never addressed before. In particular, we looked at the role of F-actin, a major player in this model system of spindle positioning during subsequent oocyte asymmetric divisions[13–17].

An assay for nucleus positioning

We used oocytes from formin 2 knockout females (hereafter *Fmn2*$^{-/-}$), whose internal symmetry is broken by their off-centred nuclei[14,17]. *Fmn2*$^{-/-}$ oocytes lack cytoplasmic microfilaments, involved in positioning of the spindle to the cortex during the first asymmetric meiotic division[15,16]. We wondered whether off-centred nuclear position in *Fmn2*$^{-/-}$ oocytes could be related to the absence of microfilaments. We designed a simple assay to reintroduce a mesh in these cells (Fig. 1a): we injected formin 2 at endogenous levels, where, if allowed to resume meiosis, 77% oocytes succeed in asymmetric division[17]. The reappearance of the actin mesh, observed by spinning-disc video microscopy using the F-actin probe GFP–UtrCH (ref. 18), starts 30 min after injection (Fig. 1b). Tracking

[1]CIRB, Collège de France, and CNRS-UMR7241 and INSERM-U1050, Equipe Labellisée Ligue Contre le Cancer, Paris F-75005, France. [2]Institut Curie, Centre de Recherche, Laboratoire Physico-Chimie, Paris F-75248, France. [3]CNRS-UMR168, Paris F-75248, France. [4]UPMC, 4 Place Jussieu, Paris F-75005, France. [5]UMR7600-CNRS/UPMC, 4 Place Jussieu, Paris F-75005, France. [6]Department of Chemical Physics, Weizmann Institute of Science, Rehovot 76100, Israel. [7]These authors contributed equally to this work. [8]Correspondence should be addressed to M-H.V. (e-mail: marie-helene.verlhac@college-de-france.fr)

Received 19 August 2014; accepted 9 February 2015; published online 16 March 2015; DOI: 10.1038/ncb3131

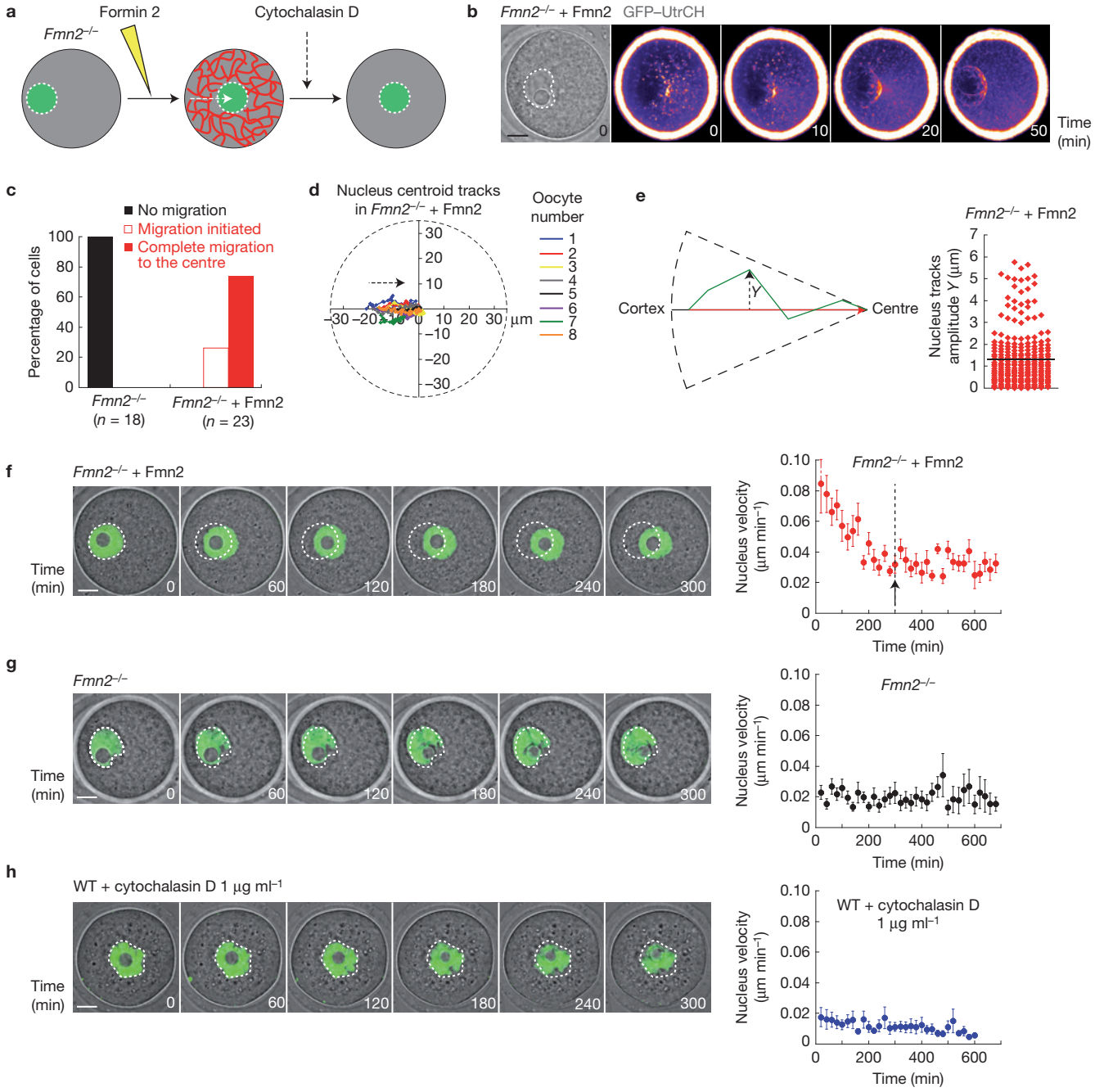

Figure 1 A cytoplasmic actin meshwork nucleated by formin 2 involved in nucleus positioning. (**a**) Microfilaments drive nucleus motion to the oocyte centre, but not its maintenance. Microfilaments (red), nucleus (green). (**b**) *De novo* formation of microfilaments. GFP–UtrCH always labels microfilaments (projection of 5 *z*-stacks separated by 5 μm). The first plane is taken 20 min after injection. Images show a representative example of nine oocytes imaged. (**c**) Percentage of migrating nuclei. $n=18$ oocytes for $Fmn2^{-/-}$ and $n=23$ oocytes for $Fmn2^{-/-}$ +Fmn2. (**d**) Trajectories of nucleus centroid. The dashed circle marks the oocyte boundaries. The black dashed arrow represents the direction of nucleus movement. Trajectories of 8 representative nuclei. (**e**) Directionality of nucleus movement. Left: scheme of the method used to address the nucleus directionality. Right: amplitude *y* (in μm) of nucleus tracks in $Fmn2^{-/-}$ oocytes injected with formin 2 from Fig. 1d. *y* values are plotted (red diamonds) and artificially separated into columns for clarity. $n=8$ oocytes. (**f**) Nucleus repositioning assay. Left: images from a video of a $Fmn2^{-/-}$ oocyte injected with cRNAs coding for formin 2 and the nuclear probe Rango (merged in green). The first plane is taken around 60 to 120 min after injection. Right: mean velocities of nucleus centroid (in μm min^{-1}) as a function of time. Black arrow at 300 min points out the end of nucleus movement, where the velocity stabilizes. $n=10$ oocytes; error bars show s.e.m. (**g**) Nucleus stays off-centred in $Fmn2^{-/-}$ oocytes. Left: images from a video of an $Fmn2^{-/-}$ oocyte injected with Rango (merged in green). Right: mean velocities of nucleus centroid as a function of time. $n=10$ oocytes; error bars show s.e.m. (**h**) Nucleus remains central in WT oocytes after cytochalasin D treatment. Left: images from a time-lapse video of a WT oocyte injected with Rango (merged in green) and treated with cytochalasin D. Right: mean velocities of nucleus centroid (in μm min^{-1}) as a function of time. $n=13$ oocytes; error bars show s.e.m. Data shown represent one out of three independent experiments in **b**. Data in **c**–**h** are aggregated from two independent experiments. Scale bars, 15 μm.

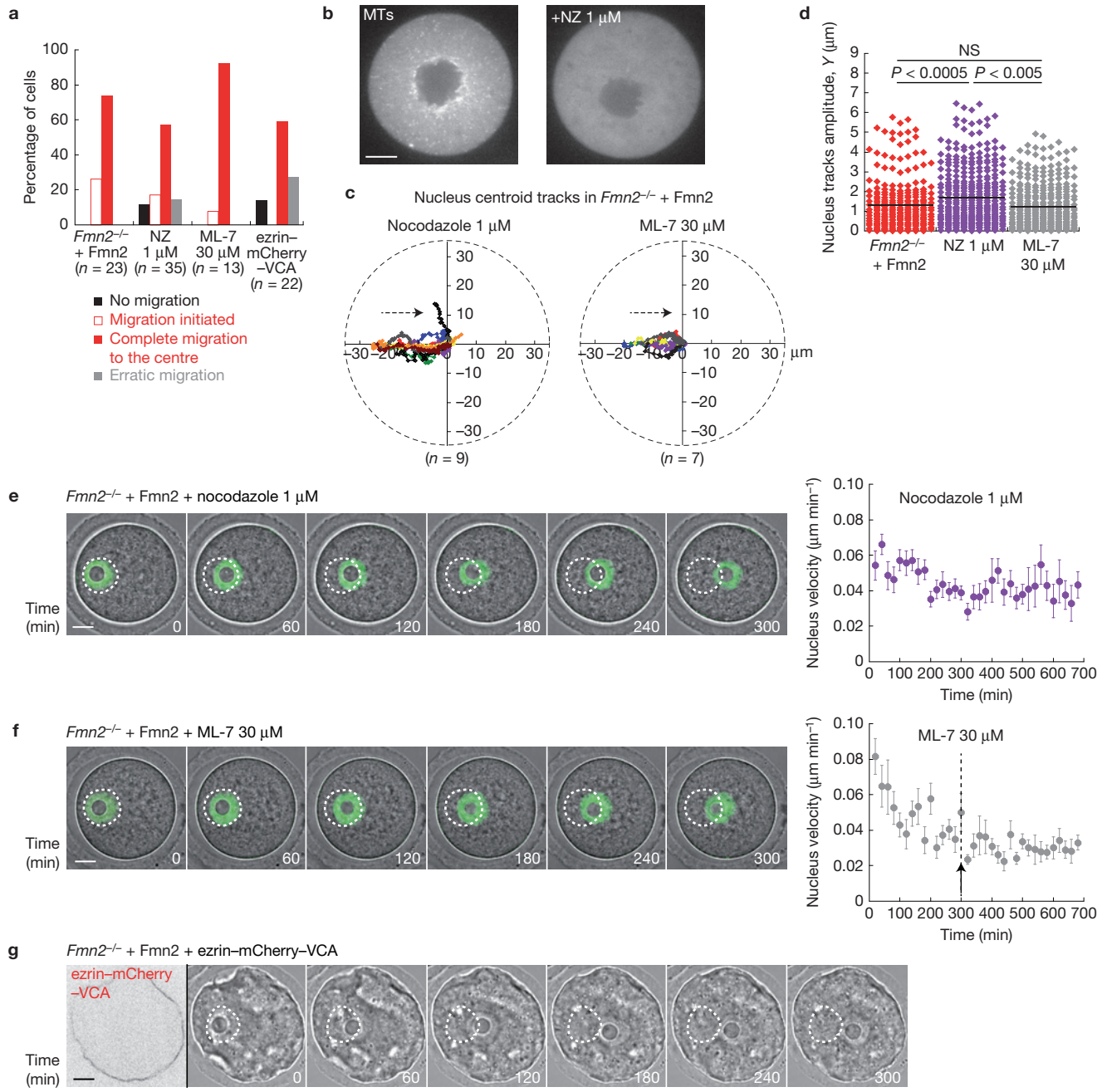

Figure 2 Microtubules and myosin II are not involved in nucleus positioning. (**a**) Percentage of migrating nuclei, on treatment with nocodazole or ML-7, or co-injected with ezrin–mCherry–VCA. The numbers of oocytes analysed are indicated in the figure. (**b**) Microtubule (MTs) organization after nocodazole treatment (right). Oocytes express the EB3–GFP marker of microtubule (+) ends. Single medial plane. Images represent one out of 15 (untreated) or 18 (treated) oocytes, respectively. (**c**) Trajectories of nucleus centroid, on treatment with nocodazole (left panel) or ML-7 (right panel). The dashed circle corresponds to oocyte boundaries. The black dashed arrow represents the direction of nucleus movement. Trajectories of 9 nuclei for nocodazole and 7 for ML-7. Note 2 off-centre nuclei (black and orange tracks) in nocodazole. (**d**) Trajectories of nucleus centroid are less directional in nocodazole. Amplitude *y* (in μm), as in Fig. 1e, of nucleus tracks in *Fmn2*$^{-/-}$ oocytes injected with formin 2, untreated or treated with nocodazole or ML-7. $n=8$ oocytes for *Fmn2*$^{-/-}$ +Fmn2, $n=9$ oocytes for nocodazole and $n=7$ oocytes for ML-7. Statistics source data for **d** can be found in Supplementary Table 1. NS, not significant. (**e**) Nucleus repositioning on nocodazole treatment. Left: images from a video of an *Fmn2*$^{-/-}$ oocyte injected with Rango (merged in green). Right: mean velocities of nucleus centroid (in μm min^{-1}) as a function of time. $n=15$ oocytes; error bars show s.e.m. (**f**) Nucleus repositioning on ML-7 treatment. Left: images from a video of an *Fmn2*$^{-/-}$ oocyte injected with formin 2 and Rango (merged in green). Right: mean velocities of nucleus centroid (in μm min^{-1}) as a function of time. Black arrow points out the end of nucleus movement, where the velocity stabilizes. $n=8$ oocytes; error bars show s.e.m. (**g**) Nucleus repositioning after cortex softening. Images from a video of an *Fmn2*$^{-/-}$ oocyte injected with formin 2 and ezrin–mCherry–VCA. The first image shows cortical localization of ezrin–mCherry–VCA. Data represent 1 out of 22 oocytes imaged. Data are aggregated from two independent experiments for *Fmn2*$^{-/-}$ +Fmn2 and ML-7, three independent experiments for nocodazole and two independent experiments for ezrin–mCherry–VCA in **a** and **c**–**f**. Data shown represent one out of two independent experiments in **b** and **g**. Scale bars, 15 μm.

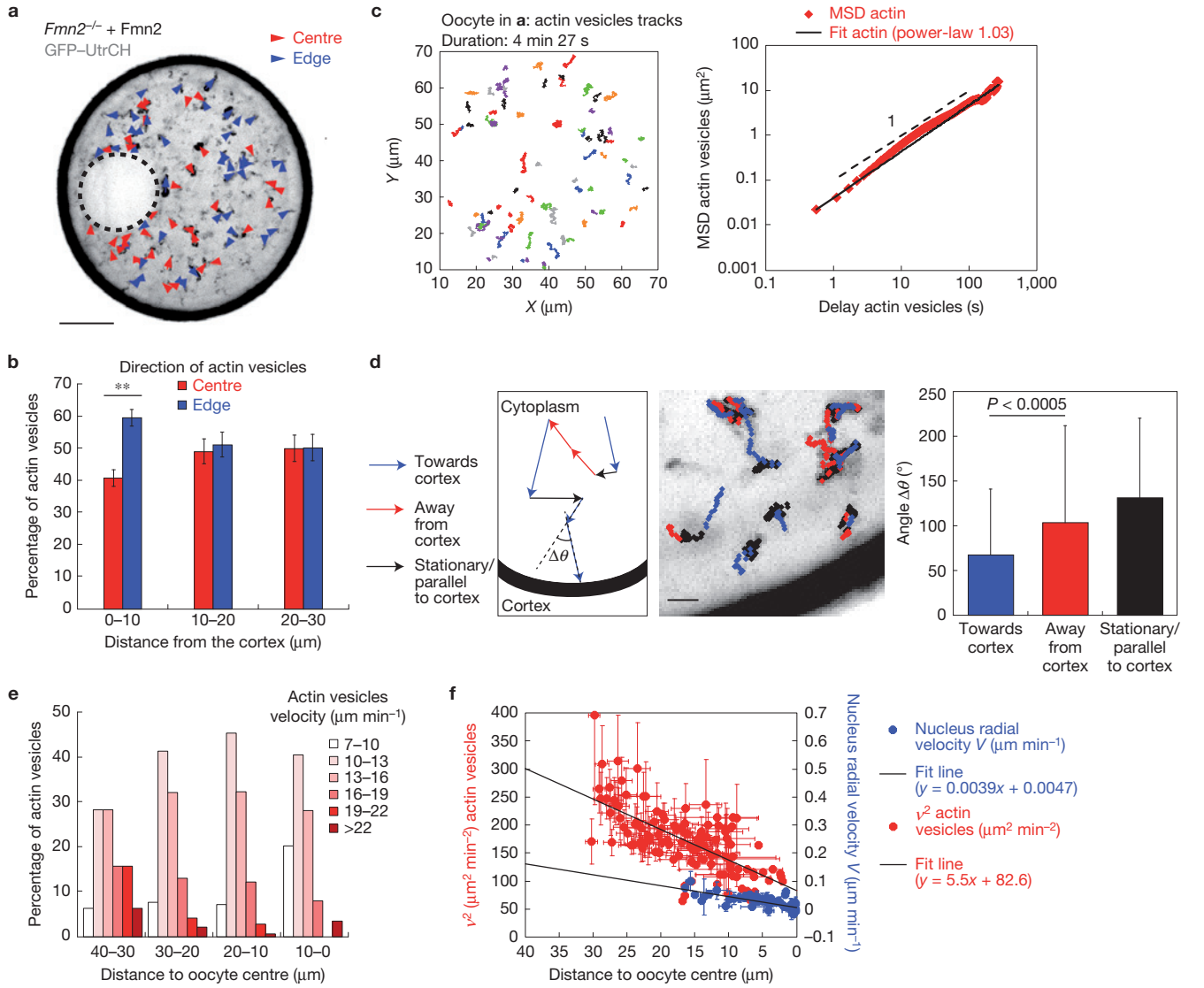

Figure 3 Actin vesicle dynamics. (**a**) Directions of actin-positive vesicles during nucleus movement. One video time projection. Dashed circle marks nucleus. Arrowheads: vesicle heading towards (red) or away from centre (blue). Scale bar, 15 μm. (**b**) No direction for actin vesicles, except close to cortex. Proportion of actin vesicles heading to centre or edge as a function of distance from cortex. Note the region close to cortex where vesicles go towards the edge (**P value for Student's t-test = 0.0074). $n = 8$ oocytes; error bars show s.e.m. (**c**) Diffusive-like motion of actin vesicles. Left: Tracks of actin vesicles during nucleus movement from the oocyte in **a**. Graph: MSD of actin vesicles is fitted as a function of time t to a power-law model $f(t) = at^b$, yielding $a = 0.04$ and $b = 1.03$, with a correlation coefficient $r^2 = 0.9308$. 597 vesicles in 8 oocytes. (**d**) Cortical attraction of actin vesicles. Directionality of vesicle tracks according to their direction relative to the cortex (blue, towards; red, away; black, stationary or parallel). $\Delta\theta$ is the angle in degrees (°) between two consecutive segments within a track (see Methods). $n = 307$ angles $\Delta\theta$ towards cortex, 241 angles $\Delta\theta$ away from cortex and 912 angles $\Delta\theta$ stationary/parallel to cortex; error bars show s.d. Statistics source data for **d** can be found in Supplementary Table 1. Scale bar, 2 μm. (**e**) Faster-moving vesicles close to cortex. Proportion of actin vesicles from categories of increasing velocities as a function of the distance to centre. $n = 597$ vesicles monitored in a total of 8 oocytes. (**f**) Actively diffusing actin vesicles establish an activity gradient. Red: mean plot of squared velocities of actin vesicles v^2 (in μm² min⁻²) as a function of the distance to the centre. Blue: mean plot of nucleus radial velocities V (in μm min⁻¹) as a function of the distance to the centre. $n = 8$ oocytes. Error bars show s.e.m. Details for correlation analysis and fitting to a linear model for **f** can be found in statistics source data in Supplementary Table 1. For actin vesicles, data are aggregated from five independent experiments in **b**,**c**,**e** and **f** and from two independent experiments in **d**. For nucleus radial velocity, data are aggregated from two independent experiments.

the position of the nucleus centroid, using a nuclear probe, Rango[19], after injection of formin 2 into *Fmn2*$^{-/-}$ oocytes, revealed a nuclear movement from the cortex towards the centre within 5 h, and its maintenance at this central location (Fig. 1d,f and Supplementary Videos 1 and 15). This movement is not due to the injection itself: *Fmn2*$^{-/-}$ oocytes injected only with Rango do not reposition their nuclei (Fig. 1c,g and Supplementary Video 2). The movement of the nucleus is directional towards the oocyte centre and spans up to 25 μm, depending on its initial position (Fig. 1d). It is confined within a lane of 6 μm, attesting to its directionality (Fig. 1e). The nucleus centroid velocity decreases from 0.08 μm min^{-1} to 0.03 μm min^{-1} after 300 min, when nuclei reach the centre (arrow in the graph in

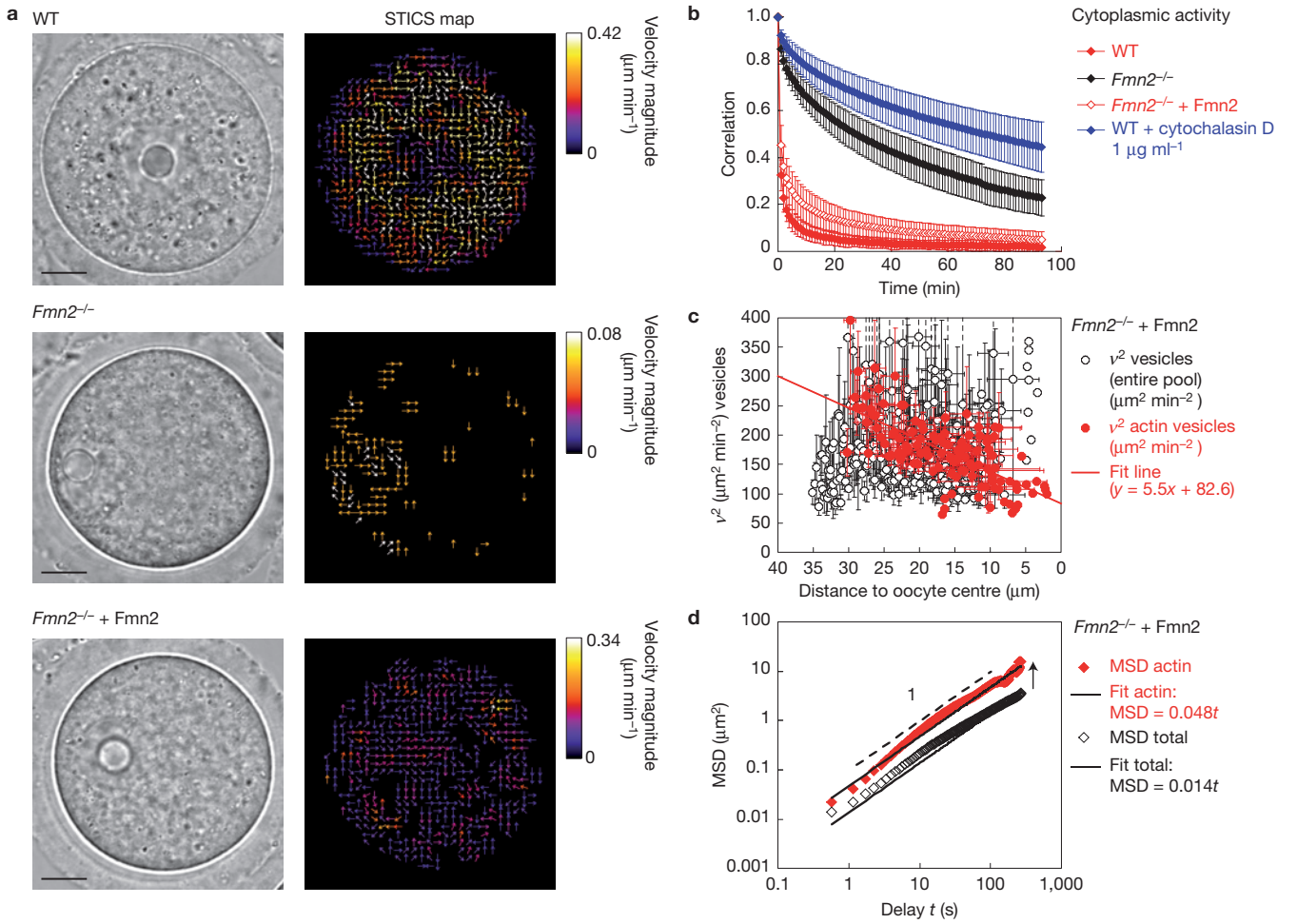

Figure 4 The cytoplasmic actin meshwork generates global cytoplasmic activity. (**a**) Reintroducing microfilaments restores cytoplasmic activity. Vector maps of cytoplasmic flows from a transmitted-light video obtained using STICS analysis. Top to bottom: WT, *Fmn2*$^{-/-}$ and *Fmn2*$^{-/-}$+Fmn2. Heat bar unit in micrometres per minute. Scale bars, 15 μm. (**b**) Image correlation analysis of cytoplasmic activity in WT, *Fmn2*$^{-/-}$, *Fmn2*$^{-/-}$+Fmn2 and WT oocytes treated with cytochalasin D. Correlations are calculated from videos of 1 min frame interval. Higher values on the *y* axis correspond to lower activity. WT: $n=53$ regions collected over 14 oocytes; *Fmn2*$^{-/-}$: $n=22$ regions, 8 oocytes; *Fmn2*$^{-/-}$ +Fmn2: $n=42$ regions, 14 oocytes; WT + cytochalasin D: $n=41$ regions, 19 oocytes. Error bars show s.d. between regions. (**c**) The activity profile of the total vesicles pool is not consistent with a pressure gradient driving nucleus movement. Red: mean plot of squared velocities of actin vesicles v^2 (in μm^2 min^{-2}) as a function of distance to oocyte centre. For a detailed description, see the legend of Fig. 3f. Black and white: mean plot of squared velocities of total vesicles v^2 (in μm^2 min^{-2}) as a function of distance to oocyte centre. $n=10$ oocytes. Error bars show s.e.m. Details for correlation analysis and fitting to a linear model for **c** can be found in statistics source data in Supplementary Table 1. (**d**) Actin and total vesicles motions undergo distinct regimes during nucleus movement. MSD of actin vesicles (red) and total vesicles (black and white). Approximate power-law slope of 1 is indicated. The arrow represents the shift between total and actin vesicles plots corresponding to a MSD ratio of 3.4. MSD data are fitted to a straight line, yielding MSD = 0.048*t* for actin vesicles and MSD = 0.014*t* for total vesicles. Actin vesicles: 597 vesicles in 8 oocytes; total vesicles: 1,956 vesicles in 10 oocytes. Data are aggregated from one experiment for WT and *Fmn2*$^{-/-}$ and two independent experiments for *Fmn2*$^{-/-}$ +Fmn2 and WT + cytochalasin D in **b**. For actin vesicles, data are aggregated from five independent experiments and for total vesicles from two independent experiments in **c** and **d**.

Fig. 1f). This non-zero basal velocity mostly reflects the variation in the centroid position due to changes in nuclear shape, nuclear membrane of mouse oocytes being deformable[20]. Nucleus movement in mouse oocytes is therefore in the lower range of known nuclear velocities[7]. The mechanism of nucleus positioning to the centre is very robust, because all *Fmn2*$^{-/-}$ oocytes injected back with formin 2 underwent nucleus movement, 74% of them making it to the centre and 26% only initiating it during the 11 h of video duration (Fig. 1c). Delayed nuclear positioning is independent of possible lower levels of formin 2 because nuclear position does not correlate with formin 2 expression (Supplementary Fig. 1). Other factors may be limiting, for example, endogenous levels of other nucleators, such as Spire 1 and 2 (ref. 21). Thus, microfilaments in mouse oocytes underlie an efficient mechanism able to drive the movement of a large organelle and its stabilization at the cell centre.

Actin is not required for nucleus maintenance

Nuclei remained centred in the absence of microfilaments (Fig. 1h left and Supplementary Video 3) with no centroid motion (Fig. 1h right). Actin is not required to maintain the nucleus in its central location, but necessary only to drive its motion from periphery to centre (Fig. 1a).

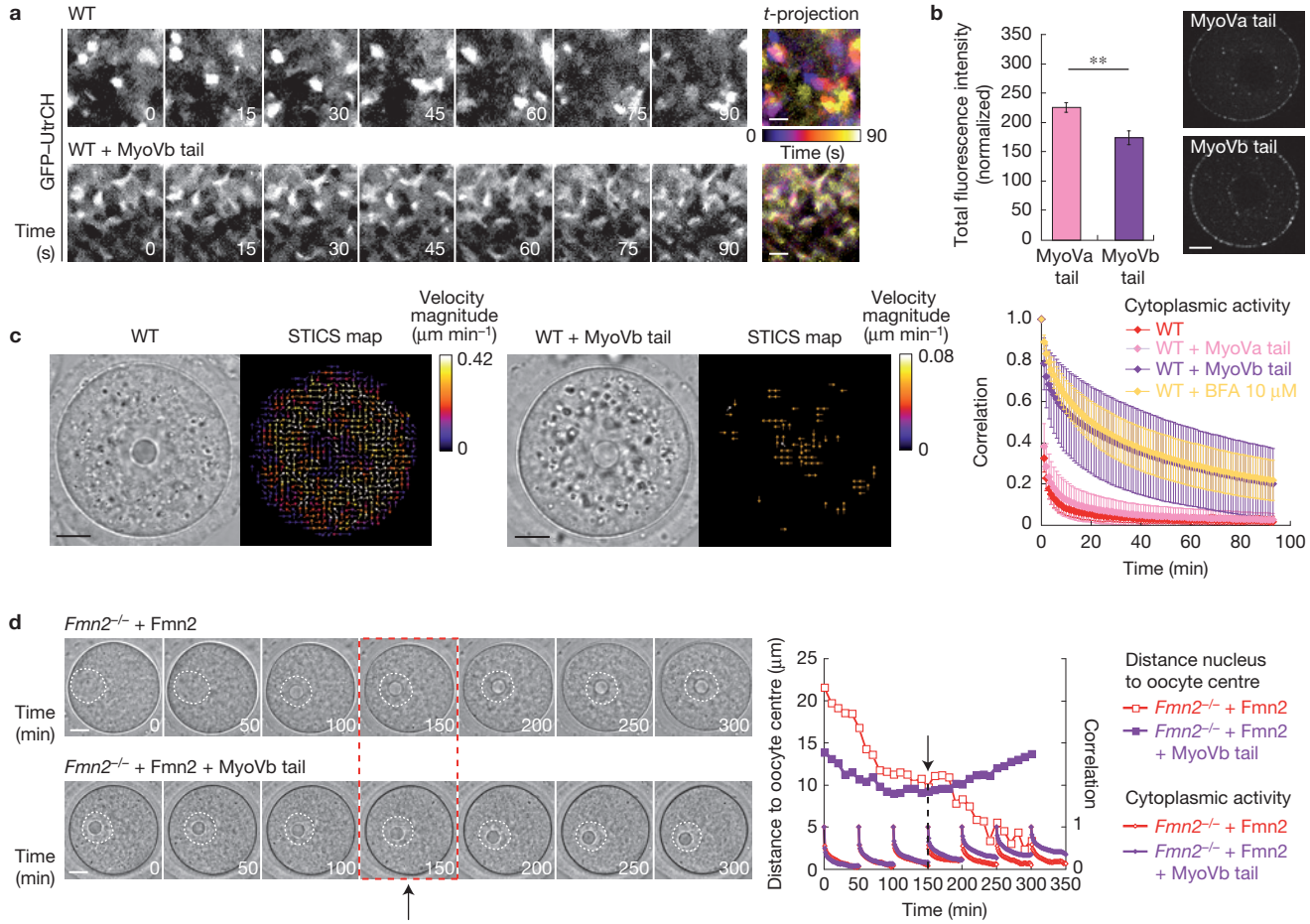

Figure 5 Cytoplasmic activity and nucleus movement require myosin Vb. (**a**) The dominant-negative tail of myosin Vb (MyoVb tail) impairs actin dynamics. Images from videos of microfilaments in WT oocytes expressing (bottom) or not (top) the MyoVb tail and their pseudo-coloured *t*-projections. Scale bars, 2 μm. Time in seconds. Heat bar unit in seconds. Data represent one out of 7 oocytes (WT) or 23 (WT + MyoVb tail) oocytes respectively. (**b**) Left: Expression levels of MyoVa and MyoVb tails. $^{**}P$ value for Mann–Whitney test = 0.0013. MyoVa tail: $n = 21$ oocytes; MyoVb tail: $n = 15$ oocytes. Error bars show s.e.m. Right: mCherry–MyoVa tail (top) and mCherry–MyoVb tail (bottom) share similar localization patterns, at the cortex and on actin vesicles. Cells are scaled similarly. Single medial plane. Scale bar, 15 μm. (**c**) The dominant-negative tail of myosin Vb impairs cytoplasmic activity. Left: vector maps of cytoplasmic flows in a WT expressing (right) or not (left) the MyoVb tail from a transmitted-light video analysed by STICS. Heat bar unit in μm min^{-1}. Scale bars, 15 μm. Graph: image correlation analysis of cytoplasmic activity in WT oocytes, untreated, MyoVa or MyoVb tail expressing, or treated with BFA. Correlations are calculated from 1 min frame interval videos. Higher values on *y* axis correspond to lower activity. WT: $n = 53$ regions collected over 14 oocytes; WT + MyoVa tail: $n = 84$ regions, 21 oocytes; WT + MyoVb tail: $n = 56$ regions, 15 oocytes; WT + BFA: $n = 61$ regions, 16 oocytes. Error bars show s.d. between regions. (**d**) Nucleus movement correlates with cytoplasmic activity. Left: images from a time-lapse video of an *Fmn2*$^{-/-}$ oocyte injected with formin 2 (top) or formin 2 and MyoVb tail (bottom). White dashed circles mark nucleus. Black arrow at 150 min and red dashed outline mark the point where nucleus path towards centre is interrupted for the oocyte expressing the MyoVb tail. Scale bars, 15 μm. Graph: from the images from the videos on the left, distance to centre and image correlations performed at successive 50 min intervals plotted as a function of time. Black arrow marks the arrest of nucleus path towards centre (purple squares plot) concomitant with decrease in cytoplasmic activity (purple activity plots). Data represent 1 out of 21 (control) and 29 (MyoVb tail) oocytes, respectively. Data shown represent one out of three independent experiments in **a** and **d**. Data are aggregated from one experiment for WT and two independent experiments for WT + MyoVa and b tails and WT + BFA in **b** and **c**.

Microtubules are not involved in nucleus positioning

Microtubules control various types of nuclear movement, alone or together with acto-myosin contractility[7]. Nocodazole induces the disappearance of interphasic microtubules (Fig. 2b; compare left and right images) yet has no major effect on nucleus migration (Fig. 2a,e and Supplementary Video 4), 75% of oocytes exhibiting migrating nuclei (Fig. 2a). A small population (14%) undergoes 'erratic nucleus movement' (Fig. 2a), corresponding to a less directional migration (Fig. 2c,d) and an inability to keep a central position (Fig. 2c). This may contribute to a slower decrease and non-stabilization of the nucleus centroid velocity curve (Fig. 2e). Similarly, treatment with nocodazole and cytochalasin D does not allow nucleus movement at steady state (Supplementary Fig. 2). Microtubules have a thus minor contribution in nucleus movement. Yet, nuclei of oocytes are surrounded by big acentriolar microtubule-organizing centres, sites for microtubule nucleation[20] (Fig. 2b), which could act as a grip for microfilaments, favouring directionality. An over-stabilized microtubule network, using Taxol (Supplementary Fig. 3b), does impede nucleus movement (Supplementary Fig. 3a,d and Supplementary Video 5). An interplay between actin and microtubules is not unexpected, existing

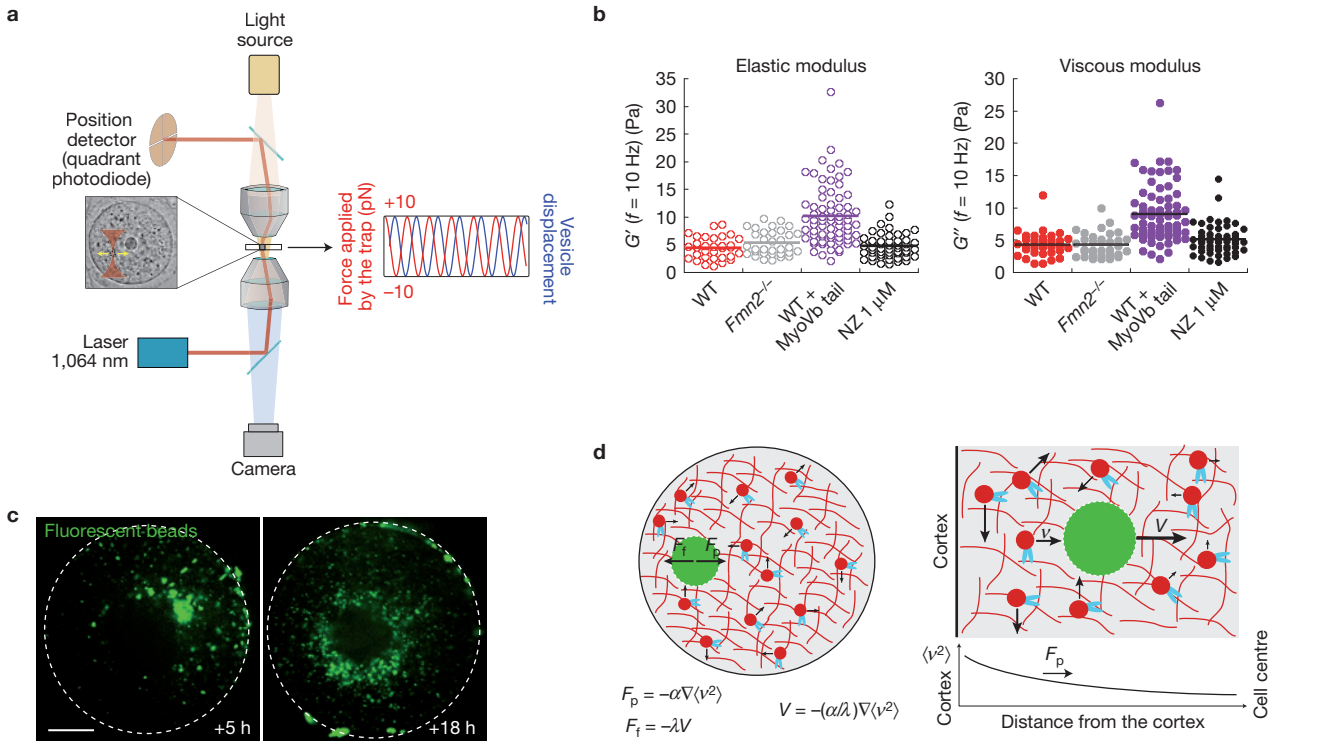

Figure 6 A model for nucleus positioning relying on a pressure gradient and cytoplasm fluidization. (**a**) Optical tweezer system to measure mechanical properties of the oocyte cytoplasm. A sinusoidal force was applied to trapped vesicles and the displacement was measured to calculate elastic and viscous moduli. (**b**) Measurements of mechanical properties by optical trapping reveal a major contribution of active diffusion in reducing cytoplasmic viscosity. Elastic (G') and viscous (G'') moduli are measured in pascals at 10 Hz in WT, *Fmn2*$^{-/-}$, WT oocytes expressing the MyoVb tail and on nocodazole treatment. WT: $n=32$ vesicles in 11 oocytes; *Fmn2*$^{-/-}$: $n=33$ vesicles in 10 oocytes; WT + MyoVb tail: $n=69$ vesicles in 23 oocytes; WT + nocodazole: $n=52$ vesicles in 8 oocytes. The mean is indicated in the figure. Statistics source data for **b** can be found in Supplementary Table 1. (**c**) Localization of fluorescent beads in oocytes 5 h (left) and 18 h (right) after injection. At 5 h, individual beads invade the whole cytoplasm whereas large aggregates remain on one side of the cell, close to the injection site. At 18 h, most of the beads are clustered at the oocyte centre, close to nuclear envelope. Images represent 1 out of 17 oocytes analysed. Scale bar, 15 µm. (**d**) Main ingredients of the physical mechanism of nucleus positioning. The nucleus experiences a propulsion force $F_p = -\alpha\nabla\langle v^2\rangle$ (α being constant) resulting from a gradient of myosin-Vb-dependent activity of actin vesicles $\langle v^2\rangle$. The propulsion force is balanced by a viscous friction force $F_f = -\lambda V$ that depends on the viscosity of the cytoplasm (λ). From $F_p + F_f = 0$, the velocity of the nucleus can be expressed as: $V = -(\alpha/\lambda)\nabla\langle v^2\rangle$. The activity v^2 can be plotted as a quadratic function of the distance to oocyte centre. The gradient of activity $\nabla\langle v^2\rangle$ vanishes close to the centre, thus keeping the nucleus in a central position. Nucleus (green); actin vesicles (red dots); actin filaments (red lines); blue: myosin Vb (blue). Data are aggregated from three independent experiments for WT and *Fmn2*$^{-/-}$, four independent experiments for WT + MyoVb tail and two independent experiments for WT + nocodazole in **b**. Data shown represent one out of two independent experiments in **c**.

later in meiosis I, in the form of an actin cage surrounding the spindle[15].

Myosin II is not involved in nucleus positioning

Acto-myosin contractility, in particular myosin II localized at spindle poles, is essential for spindle migration to the oocyte cortex during meiosis I (refs 16,22). Treatment with ML-7, an inhibitor of the myosin II activator MLCK, which inhibits spindle migration[16,22], or treatment with blebbistatin, an inhibitor of myosin II, had no effect on nucleus movement (Fig. 2a,c,d,f and Supplementary Fig. 3a,c and Supplementary Videos 6 and 7). Cortical myosin II is expelled from the cortex by an Arp2/3-dependent cortex thickening occurring later during meiosis I (ref. 22) or that can be ectopically induced in prophase I (ref. 23). In the latter, the cell cortex is softened and deformed (Fig. 2g, see cortical deformations); nevertheless, nucleus positioning still occurs in 60% of cases to the geometric centre of the oocyte (Fig. 2a,g and Supplementary Video 8). Together, these data exclude a contribution of myosin II contractility to nucleus movement.

Cortical attraction of actin filaments

Actin polymerization and actin flows could explain nuclear movement[7–9]. Analysis of high-frequency video microscopy does not allow detection of actin flows (Supplementary Fig. 4a), but highlights the dynamics of the meshwork (Supplementary Videos 9 and 10). The meshwork is made of linear microfilaments and vesicles (hereafter 'actin vesicles'). Filaments are nucleated at the surface of vesicles, which in turn move on actin tracks, making the structure highly dynamic[15,16,21]. The tracking of actin vesicles points out a mean velocity of $13.5 \pm 3.3\,\mu m\,min^{-1}$, close to the reported $12.8 \pm 3.4\,\mu m\,min^{-1}$ (ref. 21). The mean squared displacement (MSD) represents the space explored by vesicles in a given time interval and is obtained by averaging the square of the distance travelled by vesicles. The MSD plot follows a power law of 1.03, corresponding to a slope close to 1 on a log–log scale, suggesting a diffusive motion (Fig. 3c). Hence, the movement of actin vesicles is 'diffusive-like'. Tracking did not reveal any preferential direction for these actin vesicles that could explain the centripetal movement of the nucleus, besides a region

of 10 μm adjacent to the cortex where actin vesicles exhibit cortical attraction, probably due to the high density of subcortical actin (Fig. 3a,b,d). Analysis of velocity distribution across the cytoplasm highlights the appearance of a population of faster-moving vesicles close to the cortex (Fig. 3e). Accordingly, the squared velocities v^2 of actin vesicles decrease with the distance to the oocyte centre and establish a clear gradient (Fig. 3f). We developed a mathematical model to determine whether this gradient could be involved in nucleus movement.

Modelization based on a pressure gradient

In statistical fluid mechanics, v^2 is a measure of thermal agitation. In our system, we can approximate thermal agitation to the activity of actin vesicles. Using this analogy, the v^2 gradient of actin vesicles across the cytoplasm corresponds to a gradient of activity, where agitation (v^2) is highest close to the cortex. The pool of actin vesicles can be described as an assembly of particles in a fluid, whose motor-induced activity results in forces randomly kicking on the nucleus. According to statistical fluid mechanics, this activity induces an effective pressure on the nucleus $P_e \propto \rho\langle v^2\rangle$ as would do thermal agitation (ρ is the density of actin vesicles, which is constant beyond 5 μm from the cortex, Supplementary Fig. 4b). Hence, the activity gradient of actin vesicles (Fig. 3f) generates a pressure gradient and therefore a propulsion force (F_p) where $F_p = -\alpha\nabla\langle v^2\rangle$ (α being constant), capable of moving the nucleus towards the cell centre. Our model suggests that the activity gradient of actin vesicles can trigger nucleus motion within the cytoplasm.

Actin vesicles put the cytoplasm in motion

Cytoskeletal dynamics impacts the surrounding cytoplasm by dragging it along and generating cytoplasmic motion[24,25]. We wondered whether the actin meshwork would also induce cytoplasmic flows in mouse prophase I oocytes, as in *Drosophila* oocytes[25,26]. We also wondered whether the flows would contribute to nucleus movement. In the mouse, cytoplasmic streaming maintains the second meiotic spindle beneath the oocyte cortex[27] and is involved later in zygotic development[28]. Re-injecting formin 2 into the otherwise 'dormant' cytoplasm of *Fmn2*$^{-/-}$ oocytes restores cytoplasmic activity to levels close to the wild type, as shown by spatiotemporal image correlation spectroscopy[29] (STICS) and image correlation analysis (Fig. 4a,b and Supplementary Videos 11, 12 and 13). The activity of the cytoplasm is due to microfilaments because it vanishes in wild-type (WT) oocytes treated with cytochalasin D (Fig. 4b, blue curve). The STICS map indicates that at steady state in WT oocytes, the cytoplasm does not exhibit any coherent flow pattern (Fig. 4a). Despite the randomness of these cytoplasmic movements, by tracking the total vesicle pool using the fluorescent lipid dye Nile red, we examined to what extent they may contribute to nucleus positioning. Differently from actin vesicles, the squared velocities v^2 of the total vesicle pool in the cytoplasm were distributed in the form of a cloud and their distribution could not be fitted to a line (Fig. 4c). Therefore, the total vesicle pool does not establish any activity gradient and thus cannot generate pressure on the nucleus, confirming the unique behaviour of actin vesicles compared with other vesicles in the cytoplasm.

Evidence for active diffusion of actin vesicles

The movement of actin-positive vesicles depends on the activity of myosin Vb (ref. 21). The expression of the dominant-negative tail of myosin Vb (hereafter MyoVb tail) affects the overall dynamics of microfilaments[21] (Fig. 5a). Thus, the diffusive-like motion of actin vesicles depends on the motor activity of myosin Vb and can be qualified as 'active diffusion', which, in physics, defines a random, motor-driven motion that over long times results in purely diffusive motion[24]. This description fits very well with recent reports of diffusive-like motions powered by motor-induced activity in visco-elastic environments[24]. The active diffusion of actin vesicles is highlighted when comparing the MSD plots of actin versus total vesicles pools (Fig. 4d). The MSD plot for actin vesicles is shifted up compared with the one from the total vesicle pool. The shift corresponds to an MSD ratio of 3.4 between the two populations (see black arrow in Fig. 4d). To investigate to what extent this difference in MSD ratio might be due to differences in particle size, we take advantage of the known inverse relation between the MSD and the vesicle diameter. The actual diameter difference between actin vesicles (0.95 ± 0.42 μm) and total vesicles (1.49 ± 0.83 μm) predicts an MSD ratio of 1.6 (see Methods), which is about twofold smaller than the measured ratio. Hence, the motility increase of actin vesicles cannot be explained by the size difference, suggesting that motor activity drives the motion of actin vesicles.

Myosin Vb is required for cytoplasmic flow

Expression of the MyoVb tail does not affect only the dynamics of the cytoplasmic meshwork. STICS and image correlation analysis show reduced cytoplasmic activity in oocytes expressing the MyoVb tail compared with controls (Fig. 5c and Supplementary Video 14). Strikingly, even with higher expression levels for the MyoVa (ref. 21) compared with the MyoVb tail (Fig. 5b), it had no effect on cytoplasmic activity (Fig. 5c, pink curve). Treatment of oocytes, with brefeldin A (BFA), a general traffic inhibitor, blocked cytoplasmic activity as efficiently as the MyoVb tail (Fig. 5c, compare purple and yellow curves). This is consistent with the fact that actin-positive vesicles, moved by myosin Vb, are also Rab11A positive[21]. Importantly, nucleus positioning is impaired in oocytes expressing the MyoVb tail (Fig. 5d and Supplementary Videos 15 and 16). Image correlation analysis indicates that the interrupted path of the nucleus towards the centre is concomitant with the drop in cytoplasmic activity (see black arrows in Fig. 5d). This underscores the tight relationship existing between nucleus motion and cytoplasmic activity.

Myosin Vb fluidizes the cytoplasm

Using optical trapping of vesicles (Fig. 6a), we measured the mechanical properties of the cytoplasm in different conditions: WT oocytes injected or not with the MyoVb tail, *Fmn2*$^{-/-}$ and WT oocytes treated with nocodazole (Fig. 6b). Advantageously, we are able to directly measure the native environment surrounding endogenous vesicles. The cytoplasm of oocytes is globally homogeneous because measures of elastic and viscous moduli using optical trapping in various regions of the oocyte are not significantly different (Supplementary Fig. 4c). Microtubules have no impact on the

mechanics of the oocyte cytoplasm (Fig. 6b, compare WT with or without nocodazole). The minor contribution of microtubules in nucleus positioning cannot be attributed to a modification of cytoplasmic viscosity. Oocytes injected with the MyoVb tail are significantly stiffer than WT and *Fmn2*$^{-/-}$ oocytes (Fig. 6b). Their elastic and viscous moduli differ from other samples, with higher mean values but also higher dispersion, maybe due to differences in MyoVb tail expression levels after microinjection. This stiffening could result from two maybe overlapping effects. First, the MyoVb tail increases meshwork density (Fig. 5a), which in turn leads to stiffening, as observed in entangled polymer solutions[30]. Second, by generating cytoplasmic activity, myosin Vb may fluidize the cytoplasm. We favour the second hypothesis, because it explains the surprising observation that WT oocytes are as soft as *Fmn2*$^{-/-}$, even though they contain an actin mesh. A fluidizing role for motors has been documented *in vitro*[31] and the active diffusion of actin vesicles is reminiscent of a transitory regime between purely thermal diffusion and purely motor-driven transport that induces cytoplasmic stirring *in vivo*[32]. Moreover, transport by active diffusion refers not only to directed transport driven by motors on their cytoskeletal tracks, but also to the source of transport provided by the surrounding cytoplasm in motion (fluid and intracellular compartments)[24]. Thus, myosin Vb fluidizes the cytoplasm, making it compatible with the movement of large objects such as the oocyte nucleus.

A pressure gradient moves the nucleus

We integrated these results into our fluid mechanics-based model. The motion of the nucleus results from the balance of the propulsion force (F_p) and a viscous friction force (F_f), where $F_p + F_f = 0$ or $F_p - \lambda V = 0$, where V is the velocity of the nucleus and λ is proportional to the cytoplasmic viscosity. The velocity of the nucleus is then given by: $V = -(\alpha/\lambda)\nabla\langle v^2\rangle$ (Fig. 6d). This shows that the role of myosin Vb is twofold in nucleus positioning: first, generating a gradient of activity ($\nabla\langle v^2\rangle$) responsible for the propulsion force and second providing a minimal level of activity needed to fluidize the cytoplasm reducing its viscosity (λ) to lower the friction force. The high viscosity of the cytoplasm is visible at steady state: on injection of inert fluorescent beads, large bead aggregates remain, even 5 h after injection, close to the injection site (Fig. 6c, left panel and Supplementary Video 17). The model is consistent with experimental data. Nucleus velocity is proportional to the activity gradient $\nabla\langle v^2\rangle$, and thus proportional to the derivative of the actin vesicle activity v^2. Yet the measured nucleus velocity linearly decreases with the distance to the oocyte centre (Fig. 3f), suggesting that the activity v^2 may be a quadratic function of the distance to the oocyte centre (Fig. 6d). This is compatible with the measured actin vesicles activity v^2 (Fig. 3f). The model also predicts that the propulsion force vanishes at the centre, where the activity gradient is zero (Fig. 6d), leading to stabilization of the nucleus at this location. In accordance with this model, 18 h after injection, one-third of oocytes presented fluorescent latex beads apposed to their centre, close to the nuclear envelope (Fig. 6c, right panel and Supplementary Video 18). This argues that the centring mechanism is occurring because of a nonspecific pressure gradient, which promotes centration of large objects.

DISCUSSION

By setting up and applying in the living cytoplasm of the mouse oocyte the techniques used *in vitro* to determine the properties of actin gels, including *in vivo* optical tweezers measurements, we provide the first evidence of an actin-dependent mechanism for nucleus positioning that involves neither actin flow nor myosin-II-dependent contractility but that relies on active diffusion. Several studies shed light on the role active diffusion plays in many biological processes such as intracellular transport[24,32]. It is remarkable that active diffusion can lead to the directional movement and precise positioning of such a large object, the size of a somatic cell. Moreover, this mechanism spans over very long distances (up to 25 μm), similar to some of the most efficient microtubule-dependent nuclear movements reported in the vertebrate central nervous system[7]. Actin is used here as an alternative to microtubules, which here do not form large radial asters but rather small seeds[20] poorly suited for long-range transport in large cells.

Our work gives a potential explanation why this F-actin mesh, which puts large objects to the cell centre, has to be broken at meiosis resumption, for a contractile mesh to form and induce off-centre spindle positioning during the first meiotic division[15–17,22]. Spindle movement towards the periphery occurs within 2–3 h at a mean velocity of 0.12 μm min^{-1} (ref. 13), faster than the nucleus movement we report (0.08 μm min^{-1}), maybe because the spindle moving along its long axis provides less viscous friction than a round nucleus[13]. It could be possible that some aspects of our model, such as regulation of cytoplasmic viscosity, also apply for spindle migration, because myosin Vb has been reported to play a major role in spindle migration during the first meiotic division in mouse oocytes[33].

A correlation between proper nucleus centring and successful asymmetric division has been established[34], yet it will be important to address the biological relevance of nuclear centring in this model system. □

METHODS

Methods and any associated references are available in the online version of the paper.

Note: Supplementary Information is available in the online version of the paper

ACKNOWLEDGEMENTS

We thank J-Y. Tinevez (Institut Pasteur, Paris) for sharing the resources for TrackMate and MSD analysis, J. Unruh (Stowers Institute for Medical Research, Kansas City) for sharing the resources for STICS analysis, M. Schuh (MRC Cambridge) for providing the MyoVa and Vb tail plasmids and M-E. Terret for critical reading of the manuscript. M. Almonacid is a recipient of post-doctoral fellowship from the Ligue Nationale contre le Cancer. This work was supported by a grant from the Ligue Nationale Contre le Cancer (EL/2012/LNCC/MHV). This work has received support from the Fondation Bettencourt Schueller, and support under the program 'Investissements d'Avenir' launched by the French Government and implemented by the ANR, with the references: ANR-10-LABX-54 MEMO LIFE, ANR-11-IDEX-0001-02 PSL* Research University. W.W.A. is a recipient of post-doctoral fellowships from La Fondation Pierre-Gilles de Gennes and Marie Curie Actions. M.B. is a recipient of an Axa PhD fellowship. T.B. was supported by the French Agence Nationale de la Recherche (ANR-11-JSV5-0002). N.S.G. gratefully acknowledges financial support from the ISF (grant number 580/12).

AUTHOR CONTRIBUTIONS

M.A. and M-H.V. conceived and supervised the project. M.A. performed all experiments. M.A. and M-H.V. analysed all experiments. M.A. and W.W.A. performed the optical trapping experiments. M.A., W.W.A., T.B. and M-H.V. analysed optical trapping experiments. M.B. designed the software for cytoplasmic activity analysis. P.M. assisted in image analysis. N.S.G. and R.V. designed the

mathematical model. M.A. and M-H.V. wrote the manuscript, which was seen and corrected by all the authors.

COMPETING FINANCIAL INTERESTS

The authors declare no competing financial interests.

Published online at www.nature.com/doifinder/10.1038/ncb3131
Reprints and permissions information is available online at www.nature.com/reprints

1. Tang, N. & Marshall, W. F. Centrosome positioning in vertebrate development. *J. Cell Sci.* **125,** 4951–4961 (2012).
2. Burakov, A., Nadezhdina, E., Slepchenko, B. & Rodionov, V. Centrosome positioning in interphase cells. *J. Cell Biol.* **162,** 963–969 (2003).
3. Dujardin, D. L. *et al.* A role for cytoplasmic dynein and LIS1 in directed cell movement. *J. Cell Biol.* **163,** 1205–1211 (2003).
4. Gönczy, P. Centrosomes: hooked on the nucleus. *Curr. Biol.* **14,** R268–270 (2004).
5. Etienne-Manneville, S. & Hall, A. Integrin-mediated activation of Cdc42 controls cell polarity in migrating astrocytes through PKCzeta. *Cell* **106,** 489–498 (2001).
6. Gomes, E. R., Jani, S. & Gundersen, G. G. Nuclear movement regulated by Cdc42, MRCK, myosin, and actin flow establishes MTOC polarization in migrating cells. *Cell* **121,** 451–463 (2005).
7. Gundersen, G. G. & Worman, H. J. Nuclear positioning. *Cell* **152,** 1376–1389 (2013).
8. Huelsmann, S., Ylänne, J. & Brown, N. H. Filopodia-like actin cables position nuclei in association with perinuclear actin in *Drosophila* nurse cells. *Dev. Cell.* **26,** 604–615 (2013).
9. Yam, P. T. *et al.* Actin-myosin network reorganization breaks symmetry at the cell rear to spontaneously initiate polarized cell motility. *J. Cell Biol.* **178,** 1207–1221 (2007).
10. Verlhac, M. H. & Wingman Lee, K. *Oogenesis* 291–310 (John Wiley, 2010).
11. Szollosi, D., Calarco, P. & Donahue, R. P. Absence of centrioles in the first and second meiotic spindles of mouse oocytes. *J. Cell Sci.* **11,** 521–541 (1972).
12. Halet, G. & Carroll, J. Rac activity is polarized and regulates meiotic spindle stability and anchoring in mammalian oocytes. *Dev. Cell.* **12,** 309–317 (2007).
13. Verlhac, M. H., Lefebvre, C., Guillaud, P., Rassinier, P. & Maro, B. Asymmetric division in mouse oocytes: with or without Mos. *Curr. Biol.* **10,** 1303–1306 (2000).
14. Dumont, J. *et al.* Formin-2 is required for spindle migration and for the late steps of cytokinesis in mouse oocytes. *Dev. Biol.* **301,** 254–265 (2007).
15. Azoury, J. *et al.* Spindle positioning in mouse oocytes relies on a dynamic meshwork of actin filaments. *Curr. Biol.* **18,** 1514–1519 (2008).
16. Schuh, M. & Ellenberg, J. A new model for asymmetric spindle positioning in mouse oocytes. *Curr. Biol.* **18,** 1986–1992 (2008).
17. Azoury, J., Lee, K. W., Georget, V., Hikal, P. & Verlhac, M-H. Symmetry breaking in mouse oocytes requires transient F-actin meshwork destabilization. *Development* **138,** 2903–2908 (2011).
18. Burkel, B. M., von Dassow, G. & Bement, W. M. Versatile fluorescent probes for actin filaments based on the actin-binding domain of utrophin. *Cell Motil. Cytoskeleton* **64,** 822–832 (2007).
19. Dumont, J. *et al.* A centriole- and RanGTP-independent spindle assembly pathway in meiosis I of vertebrate oocytes. *J. Cell Biol.* **176,** 295–305 (2007).
20. Luksza, M., Queguiner, I., Verlhac, M-H. & Brunet, S. Rebuilding MTOCs upon centriole loss during mouse oogenesis. *Dev. Biol.* **382,** 48–56 (2013).
21. Schuh, M. An actin-dependent mechanism for long-range vesicle transport. *Nat. Cell Biol.* **13,** 1431–1436 (2011).
22. Chaigne, A. *et al.* A soft cortex is essential for asymmetric spindle positioning in mouse oocytes. *Nat. Cell Biol.* **15,** 958–966 (2013).
23. Chaigne, A. *et al.* A narrow window of cortical tension guides asymmetric spindle positioning in the mouse oocyte. *Nat. Commun.* **6,** 6027 (2015).
24. Brangwynne, C. P., Koenderink, G. H., MacKintosh, F. C. & Weitz, D. A. Intracellular transport by active diffusion. *Trends Cell Biol.* **19,** 423–427 (2009).
25. Theurkauf, W. E., Smiley, S., Wong, M. L. & Alberts, B. M. Reorganization of the cytoskeleton during Drosophila oogenesis: implications for axis specification and intercellular transport. *Development* **115,** 923–936 (1992).
26. Gutzeit, H. O. The role of microfilaments in cytoplasmic streaming in Drosophila follicles. *J. Cell Sci.* **80,** 159–169 (1986).
27. Yi, K. *et al.* Dynamic maintenance of asymmetric meiotic spindle position through Arp2/3-complex-driven cytoplasmic streaming in mouse oocytes. *Nat. Cell Biol.* **13,** 1252–1258 (2011).
28. Ajduk, A. *et al.* Rhythmic actomyosin-driven contractions induced by sperm entry predict mammalian embryo viability. *Nat. Commun.* **2,** 417 (2011).
29. Hebert, B., Costantino, S. & Wiseman, P. W. Spatiotemporal image correlation spectroscopy (STICS) theory, verification, and application to protein velocity mapping in living CHO cells. *Biophys. J.* **88,** 3601–3614 (2005).
30. Morse, D. C. Viscoelasticity of concentrated isotropic solutions of semiflexible polymers. *Macromolecules* **31,** 7044–7067 (1998).
31. Humphrey, D., Duggan, C., Saha, D., Smith, D. & Käs, J. Active fluidization of polymer networks through molecular motors. *Nature* **416,** 413–416 (2002).
32. Fakhri, N. *et al.* High-resolution mapping of intracellular fluctuations using carbon nanotubes. *Science* **344,** 1031–1035 (2014).
33. Holubcová, Z., Howard, G. & Schuh, M. Vesicles modulate an actin network for asymmetric spindle positioning. *Nat. Cell Biol.* **15,** 937–947 (2013).
34. Brunet, S. & Maro, B. Germinal vesicle position and meiotic maturation in mouse oocyte. *Reproduction* **133,** 1069–1072 (2007).

DOI: 10.1038/ncb3131

nature cell biology

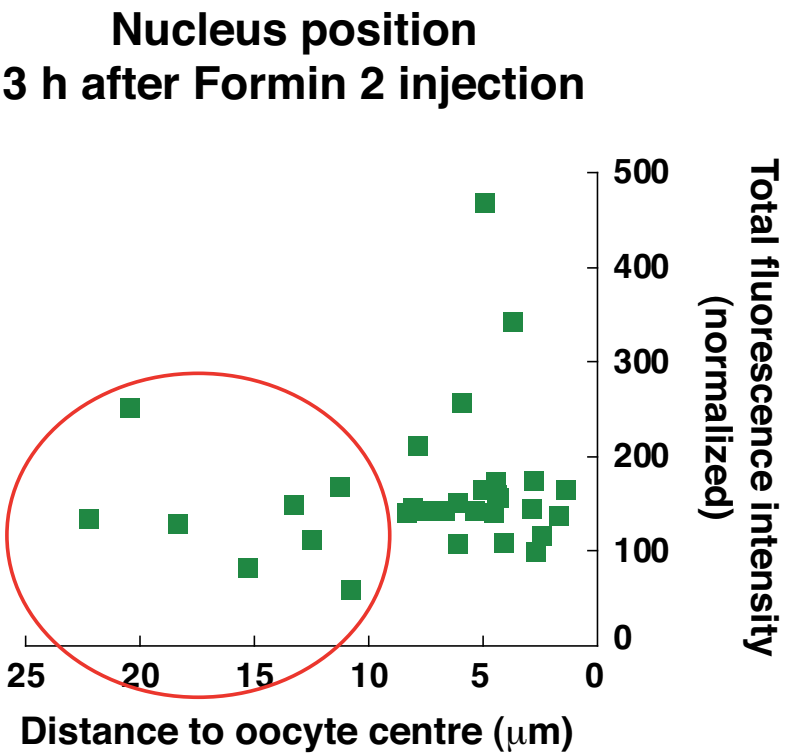

Supplementary Figure 1 Formin 2-GFP expression as a function of the position of the nucleus 3 h after injection. The red circle points out the population of oocytes with delayed nuclei. Expression levels are quantified by the integrated fluorescence intensity of Formin 2-GFP over an entire oocyte normalized by the oocyte surface (in μm^2). Correlation analysis: correlation coefficient rs=-0.1484, p-value=0.4256, indicative of the non-correlation of the data. Non-linear regression fitting to a straight line: low correlation coefficient r^2= 0.0007 makes the data incompatible with a linear model. n=31 oocytes. Data are aggregated from two independent experiments.

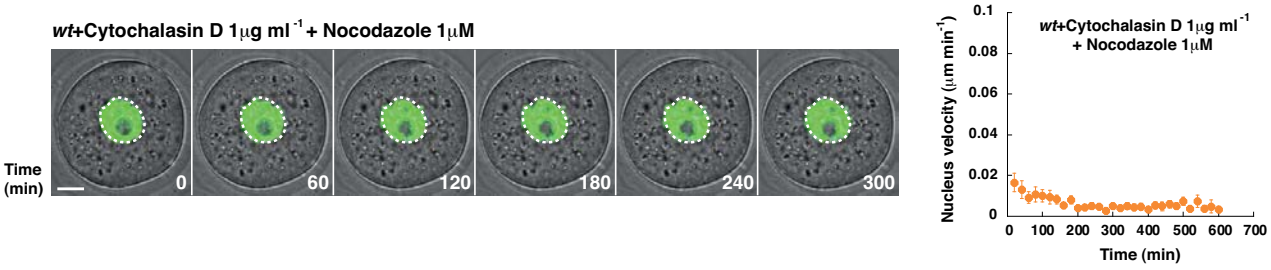

Supplementary Figure 2 Microtubules are not involved in nucleus maintenance at the centre. Nucleus remains central in *wt* oocytes after Nocodazole and Cytochalasin D treatment. Left: time-lapse movie of a *wt* oocyte injected with Rango (merged in green) and treated with Nocodazole and Cytochalasin D. Right: mean velocities of nucleus centroid (in μm min^{-1}) as a function of time. n=13 oocytes. Time is in minute, scale bar is 15 μm and error bars display SEM. Data are aggregated from two independent experiments.

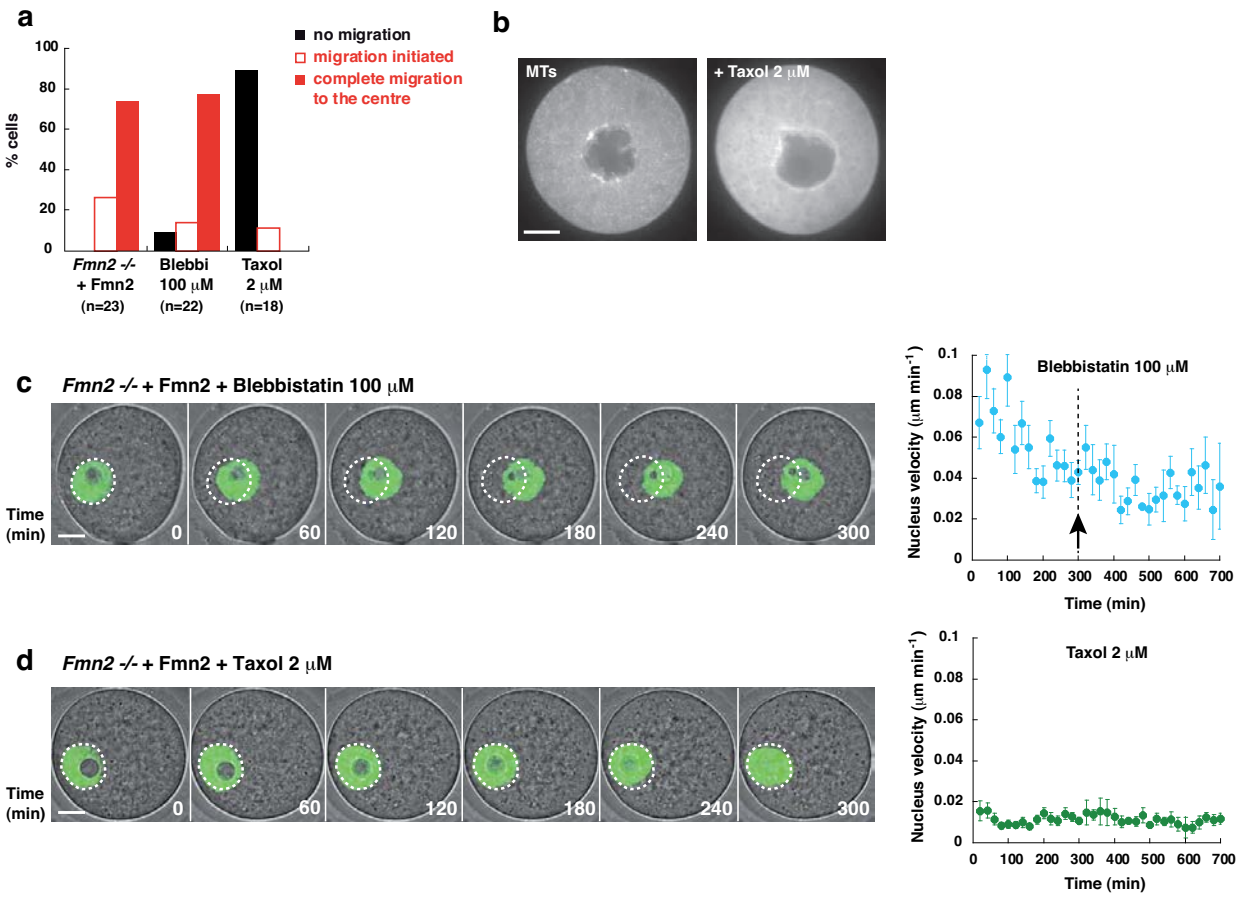

Supplementary Figure 3 Microtubules and Myosin II are not involved in nucleus positioning. a: Percentage of migrating versus non-migrating nuclei in *Fmn2 -/-* oocytes injected with Formin 2, untreated, upon treatment with Blebbistatin or Taxol. n=23 oocytes for *Fmn2 -/-* + Fmn2; n=22 oocytes for Blebbistatin, n=18 oocytes for Taxol. b: Microtubule (MTs) network organization in untreated oocytes (left) and in oocytes treated with Taxol (right). Oocytes express the marker of microtubule (+) ends EB3-GFP. Time-projections from one movie (frame interval: 357 ms, 480 frames, movie duration: 2 min 51 s), single medial plane. Please note the absence of EB3 comets in the oocyte treated with Taxol, indicative of impaired microtubule network dynamics. Untreated: n=8 oocytes, treated: n=7 oocytes. c: Nucleus repositioning following Formin 2 injection into *Fmn2 -/-* oocytes upon 100 μM Blebbistatin treatment. Left panel: time-lapse movie of an *Fmn2 -/-* oocyte injected with cRNAs coding for Formin 2 and the nuclear probe Rango (merged in green). Right panel: mean velocities of nucleus centroid (in μm min^{-1}) as a function of time. Black arrow points out the end of nucleus movement, where the velocity stabilizes. n=10 oocytes. Error bars display SEM. d: Nucleus repositioning upon Taxol treatment. Left panel: time-lapse movie of an *Fmn2 -/-* oocyte injected with cRNAs coding for Formin 2 and the nuclear probe Rango (merged in green). Right panel: mean velocities of nucleus centroid (in μm min^{-1}) as a function of time. n=13 oocytes. Error bars display SEM. Data are aggregated from two independent experiments for *Fmn2 -/-* + Fmn2, Blebbistatin and Taxol in a, c and d. Data shown represent one out of one experiment in b.

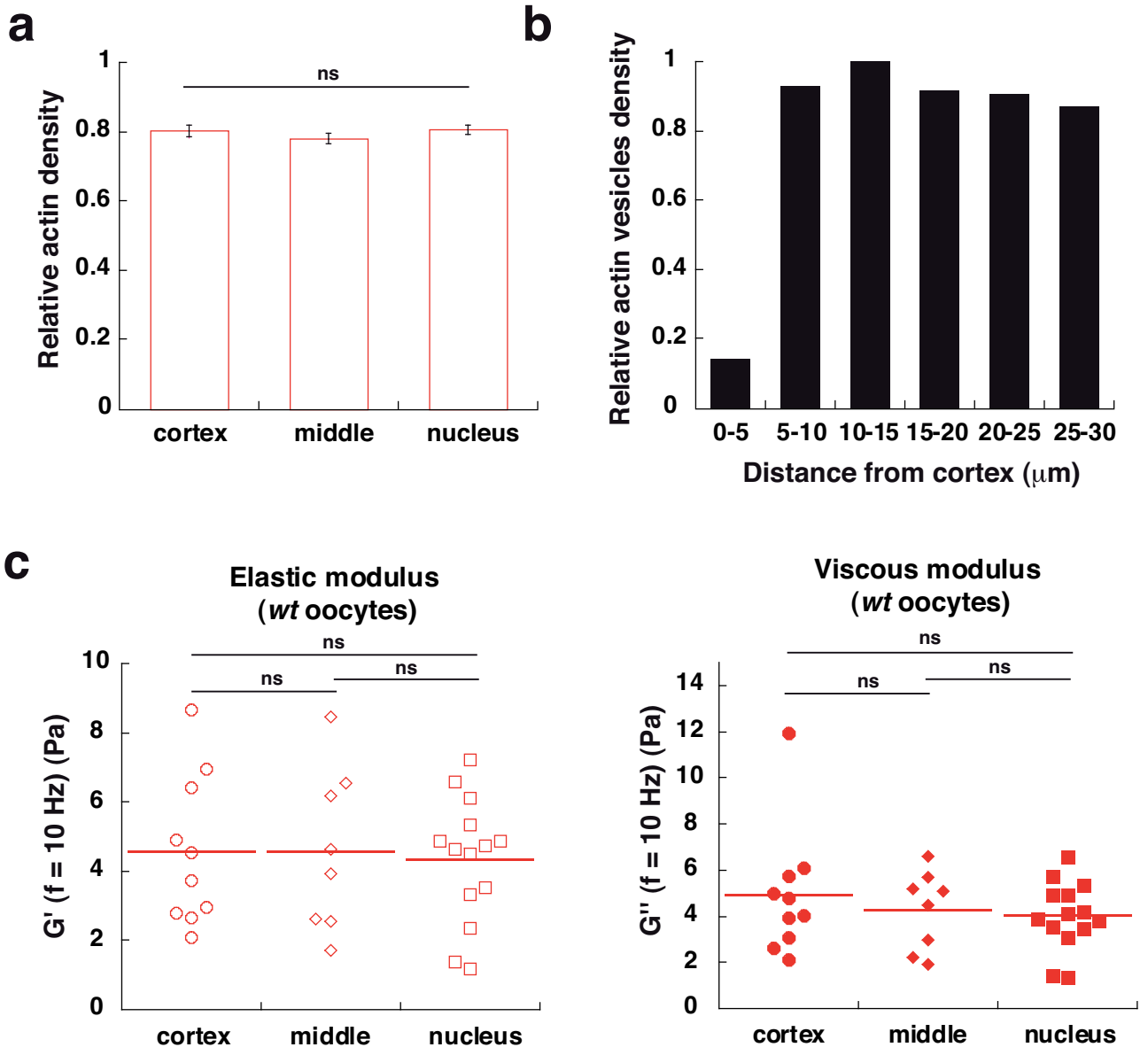

Supplementary Figure 4 Actin distribution and mechanical properties of the cytoplasm. a: No differences in actin density are detected across the cytoplasm of *Fmn2 -/-* oocytes injected with Formin 2. Actin densities are represented as the ratio of GFP-UtrCH integrated fluorescence intensities of cytoplasmic regions near the cortex, in the middle and near the nucleus normalized by the region area over integrated fluorescence intensity of the entire oocyte normalized by the oocyte surface. P-value for one-way ANOVA= 0.48. n=8 oocytes. Error bars display SEM. b: No density gradient of actin vesicles is observed in *Fmn2 -/-* oocytes injected with Formin 2. Actin vesicles density as a function of the distance from the cortex. Densities are represented as a ratio with the highest density observed in the area 10-15 μm away from the cortex (relative density of 1). n=8 oocytes. c: Direct measurements by optical trapping of mechanical properties in different regions of the cytoplasm in *wt* oocytes. Elastic (G') and viscous (G") moduli are measured in Pa at 10 Hz. Mean and SD for elastic moduli are 4.6+/-2.2 near cortex, 4.6+/-2.3 in the middle, 4.3+/-1.8 near nucleus. Mean and SD for viscous moduli are 4.9+/-2.8 near cortex, 4.3+/-1.7 in the middle, 4.0+/-1.5 near nucleus. P-values for Kolmogorov-Smirnov test for equality of distributions are 0.83 for cortex-middle, 0.98 for cortex-nucleus, 0.91 for middle-nucleus (elastic moduli); 0.98 for cortex-middle, 0.98 for cortex-nucleus, 0.72 for middle-nucleus (viscous moduli). n = 32 vesicles measured in 11 oocytes. Data are aggregated from five independent experiments in a and b and from three independent experiments in c.

Figure	Values	SEM/SD	n value	Number of experiments	Statistical test	Statistical test results
2d	Mean amplitude Y *Fmn2* -/- + Fmn2: 1.3+/-1.3 NZ: 1.7+/-1.4 ML-7: 1.2+/-1.1	SD	*Fmn2* -/- + Fmn2: n=8 oocytes NZ: n=9 oocytes ML-7: n=7 oocytes	*Fmn2* -/- + Fmn2: 2 NZ: 3 ML-7: 2	Kolmogorov-Smirnov	P-values: *Fmn2* -/- + Fmn2 vs NZ: 3.9 10^{-4} *Fmn2* -/- + *Fmn2* vs ML-7: 0.78 NZ vs ML-7: 4.2
3d	Mean absolute angle Δθ towards: 67.3+/-73.5 away: 103.7+/-107.9 stationary/parallel: 131.2+/-88.73	SD	towards: 307 angles Δθ away: 241 angles Δθ stationary/parallel: 912 angles Δθ	2	Kolmogorov-Smirnov	P-values: towards vs away: 3.10^{-4} towards vs stationary/parallel: 2.3 10^{-31} away vs stationary/parallel:
3f	v^2 actin vesicles: Correlation analysis: correlation coefficient rs= 0.65 Non-linear regression fitting to a straight line: correlation coefficient r^2= 0.47 $y_{intercept}$=82.6+/-9.4, slope= 5.5+/-0.5 Vnucleus: Correlation analysis: correlation coefficient rs= 0.70 Non-linear regression fitting to a straight line: correlation coefficient r^2= 0.57 $y_{intercept}$=0.0047+/-0.0029, slope= 0.0039+/-0.00046	SEM	v^2 actin vesicles: n=8 oocytes V nucleus: n=8 oocytes	v^2 actin vesicles: 5 Vnucleus: 2		v^2 actin vesicles: Correlation analysis: p-value <0.0001. Non-linear regression fitting to a straight line: p value for runs test = 0.12, compatible with a linear model Vnucleus: Correlation analysis: p-value <0.0001. Non-linear regression fitting to a straight line: p-value for runs test = 0.25, compatible with a linear model
4c	v^2 total vesicles: Non-linear regression fitting to a straight line: correlation coefficient r^2= 0.014	SEM	v^2 total vesicles: n=10 oocytes	v^2 total vesicles: 2		Non-linear regression fitting to a straight line: Residuals not randomly scattered above and below the X-axis and p-value for normality test of residuals (D'Agostino & Pearson test)<0.0001, incompatible with a linear model.
6b	Mean elastic moduli G': *wt*: 4.5+/-2.0 *Fmn2* -/-: 5.4+/-2.2 *wt*+MyoVb tail: 10.3+/-5.4 *wt*+NZ: 4.8 +/- 2.2 Mean viscous moduli G'': *wt*: 4.4+/-2.0 *Fmn2* -/-: 4.4+/-1.8 *wt*+MyoVb tail: 9.1+/-4.3 *wt*+NZ: 5.1+/-2.4	SD	*wt*: n=11 oocytes, 32 vesicles *Fmn2* -/-: n=10 oocytes, 33 vesicles *wt*+MyoVb tail: n=23 oocytes, 69 vesicles *wt*+NZ: n=8 oocytes, 52 vesicles	*wt*: 3 *Fmn2* -/-: 3 *wt*+MyoVb tail: 4 *wt*+NZ: 2	Kolmogorov-Smirnov	P-values: Elastic moduli G': *wt-Fmn2* -/-: 0.27 *wt-wt*+MyoVb tail: 3.69 10^{-8} *wt* *wt*+NZ: 0.88 Viscous moduli G'': *wt-Fmn2* -/-: 0.68 *wt-wt*+MyoVb tail: 4.73 10^{-10} *wt-wt*+NZ: 0.37

Supplementary Table 1 Statistics source data
This table provides detailed description of data from legends of Figures 2d, 3d, 3f, 4c and 6b.

Supplementary Video Legends

Supplementary Video 1 Nucleus repositioning upon Formin 2 injection into *Fmn2* -/- oocytes. Time-lapse movie of an *Fmn2* -/- oocyte injected with cRNAs coding for Formin 2 together with the nuclear probe Rango (in green). Frames are taken every 20 min. Movie duration is 360 min.

Supplementary Video 2 Nucleus stays off-centred in *Fmn2* -/- oocytes. Time-lapse movie of a *Fmn2* -/- oocyte injected with cRNA coding for the nuclear probe Rango (green). Frames are taken every 20 min. Movie duration is 360 min.

Supplementary Video 3 Nucleus keeps its central position in wt oocytes treated with 1μg ml^{-1} Cytochalasin D. Time-lapse movie of a *wt* oocyte injected with cRNA coding for the nuclear probe Rango (green). Frames are taken every 20 min. Movie duration is 300 min.

Supplementary Video 4 Nucleus repositioning following Formin 2 injection into *Fmn2* -/- oocytes upon 1 μM Nocodazole treatment. Time-lapse movie of an *Fmn2* -/- oocyte injected with cRNAs coding for Formin 2 together with the nuclear probe Rango (green). Frames are taken every 20 min. Movie duration is 300 min.

Supplementary Video 5 Nucleus stays off-centred in *Fmn2* -/- oocytes injected with Formin 2 upon 2 μM Taxol treatment. Time-lapse movie of a *Fmn2* -/- oocyte injected with cRNAs coding for Formin 2 together with the nuclear probe Rango (green). Frames are taken every 20 min. Movie duration is 300 min.

Supplementary Video 6 Nucleus repositioning following Formin 2 injection into *Fmn2* -/- oocytes upon 30 μM ML-7 treatment. Time-lapse movie of an *Fmn2* -/- oocyte injected with cRNAs coding for Formin 2 and the nuclear probe Rango (green). Frames are taken every 20 min. Movie duration is 300 min.

Supplementary Video 7 Nucleus repositioning following Formin 2 injection into *Fmn2* -/- oocytes upon 100 μM Blebbistatin treatment. Time-lapse movie of an *Fmn2* -/- oocyte injected with cRNAs coding for Formin 2 and the nuclear probe Rango (green). Frames are taken every 20 min. Movie duration is 300 min.

Supplementary Video 8 Nucleus repositioning in oocytes expressing Ezrin-mCherry-VCA. Time-lapse movie of an *Fmn2* -/- oocyte injected with cRNAs coding for Formin 2 and Ezrin-mCherry-VCA. Frames are taken every 1 min. Movie duration is 300 min.

Supplementary Video 9 Dynamics of the F-actin cytoplasmic meshwork during nucleus movement in an *Fmn2* -/- oocyte injected with Formin 2. Time-lapse movie of an *Fmn2* -/- oocyte injected with cRNAs coding for Formin 2 and the F-actin probe GFP-UtrCH. Frame interval: 557 ms, 480 frames, movie duration: 4 min 27s, single medial plane. This movie is used in Figures 3a and 3c for mapping vesicles directions and tracks, respectively.

Supplementary Video 10 Dynamics of the F-actin cytoplasmic meshwork during nucleus movement in an *Fmn2* -/- oocyte injected with Formin 2. Time-lapse movie of an *Fmn2* -/- oocyte injected with cRNAs coding for Formin 2 and the F-actin probe GFP-UtrCH. Frame interval: 556 ms, 480 frames, movie duration: 4 min 27s, single medial plane.

Supplementary Video 11 Cytoplasmic activity in a *wt* oocyte. Transmitted light movie. Frames are taken every 1 min. Movie duration is 49 min. This movie is used for STICS analysis in Figure 4a, top panel and Figure 5c, left panel.

Supplementary Video 12 Cytoplasmic activity in an *Fmn2* -/- oocyte. Transmitted light movie. Frames are taken every 1 min. Movie duration is 50 min. This movie is used for STICS analysis in Figure 4a, middle panel.

Supplementary Video 13 Cytoplasmic activity in an *Fmn2* -/- oocyte injected with cRNAs coding for Formin 2. Transmitted light movie. Frames are taken every 1 min. Movie duration is 50 min. This movie is used for STICS analysis in Figure 4a, bottom panel.

Supplementary Video 14 Cytoplasmic activity in a *wt* oocyte expressing the MyoVb tail. Transmitted light movie. Frames are taken every 1 min. Movie duration is 50 min. This movie is used for STICS analysis in Figure 5c, right panel.

Supplementary Video 15 Nucleus repositioning upon Formin 2 injection into *Fmn2* -/- oocytes. Time-lapse movie of an *Fmn2* -/- oocyte injected with cRNAs coding for Formin 2. Frames are taken every 1 min. Movie duration is 349 min.

Supplementary Video 16 Arrest of nucleus movement is concomitant with the drop in cytoplasmic activity in oocytes expressing MyoVb tail. Time-lapse movie of an *Fmn2* -/- oocyte injected with Formin 2 together with MyoVb tail. Frames are taken every 1 min. Movie duration is 349 min.

Supplementary Video 17 Cytoplasm of a *wt* oocyte injected with 0.1 μm latex fluorescent beads, 5 h after injection. Frame interval: 555 ms, 480 frames, movie duration: 4 min 27 s, single medial plane. The first frame of this movie is displayed in Figure 6c, left panel.

Supplementary Video 18 Cytoplasm of a *wt* oocyte injected with 0.1 μm latex fluorescent beads, 18 h after injection. Frame interval: 556 ms, 480 frames, movie duration: 4 min 27 s, single medial plane. The first frame of this movie is displayed in Figure 6c, right panel.